Creep in $0.91(Na_{1/2}Bi_{1/2})TiO_3$-$0.06BaTiO_3$-$0.03K_{0.5}Na_{0.5}NbO_3$ lead-free piezoceramic under constant electric field loads

Di Chen[1,2,*], Azatuhi Ayrikyan[3], Xiangcheng Chu[2,4], Marc Kamlah[5] and Kyle G Webber[3]

[1] Grandblue Research Institute, Grandblue Environment Co., Ltd, Ronghe Road 23, 528200 Foshan, People's Republic of China

[2] Smart Devices and High-End Equipment Lab, Foshan (Southern China) Institute for New Materials, 528247 Foshan, People's Republic of China

[3] Department of Materials Science and Engineering, Friedrich-Alexander-Universität Erlangen-Nürnberg, Martensstraße 5, 91058 Erlangen, Germany

[4] State Key Laboratory of New Ceramics and Fine Processing, School of Material Science and Engineering, Tsinghua University, 100084 Beijing, People's Republic of China

[5] Institute for Applied Materials (IAM-WBM), Karlsruhe Institute of Technology, Hermann-von-Helmholtz-Platz 1, 76344 Eggenstein-Leopoldshafen, Germany

E-mail: chendi@grandblue.cn

Abstract

This work explores the creep behavior of polycrystalline $0.91(Na_{1/2}Bi_{1/2})TiO_3$ -$0.06BaTiO_3$-$0.03K_{0.5}Na_{0.5}NbO_3$ under constant electric fields. It reveals intriguing time-dependent variations in both polarization and strain response, which can be attributed to a transformation from the relaxor state to a long-range ferroelectric order. Meanwhile, bulk volume resistivity values are obtained to eliminate the influence of leakage current on the polarization assessment. The findings provide valuable insights into the creep behavior of lead-free relaxor ferroelectrics, laying a solid foundation for enhancing the performance and reliability of piezoactuators.

Keywords: lead-free piezoceramic, constant electric field loading, creep behavior

1. Introduction

Lead-based piezoelectrics are widely used for sensors and actuators due to their intrinsic coupling between electro-mechanical, electro-optical, and thermo-electrical properties [1–3]. To date, solid solutions of lead zirconate titanate ($Pb(Zr,Ti)O_3$, PZT) remain dominant in the piezoelectric actuator market. The refinement, processing, and use of lead and lead oxide, however, raise numerous environmental and health concerns [4]. For this reason, considerable research effort has been invested into developing new lead-free ceramics over the past decades [5, 6]. Despite the promising properties of emerging lead-free compositions, the transition from PZT to lead-free materials has been met with hesitation in many industrial applications [7]. Actuators, in particular, require piezoceramics with specific properties such as large electric-field induced strain, high blocking force, and a high Curie temperature (T_C), which are closely related to the microstructure and composition [8]. The main challenges in the adoption of lead-free piezoelectrics have been discussed, including understanding fundamental mechanisms, achieving large temperature-stable piezoresponse, and designing fabrication-friendly and customizable compositions [9]. While several lead-free materials have shown excellent

* Author to whom any correspondence should be addressed.

electromechanical properties, surpassing those of lead-based counterparts [10–13], the search for a complete replacement for PZT in actuator applications remains an ongoing challenge [14]. The (1-x-y)($Na_{1/2}Bi_{1/2}$)TiO_3-x$BaTiO_3$-y$K_{0.5}Na_{0.5}NbO_3$ (NBT-BT-KNN) solid solutions have garnered significant interest for off-resonance actuator applications due to their ability to exhibit giant electric-field-induced strains [15, 16]. This remarkable property arises from a reversible electric field-induced transition between a non-polar state and a polar state [17]. To achieve this behavior, the introduction of KNN components was utilized to destabilize the long-range ferroelectric order, effectively shifting the ferroelectric-to-relaxor transition to lower temperatures, even close to or below room temperature [18]. Various investigations have shown a similar destabilization effect with other end members, such as $SrTiO_3$ [19] and $LiNbO_3$ [20]. At room temperature, the NBT-0.06BT-0.03KNN composition exists as an ergodic relaxor in a non-polar state, characterized by the absence of long-range ferroelectric order, which is evident in high-resolution transmission electron microscopy studies showing a 'grainy contrast' [21–23]. However, the application of an external electric field induces the development of domains, indicating the formation of long-range ferroelectric order. Corresponding transition from a pseudo-cubic phase to tetragonal, rhombohedral, or mixed tetragonal/rhombohedral phase depending on the composition have been revealed by means of *in situ* high energy synchrotron diffraction studies [24, 25]. *In situ* high-resolution x-ray and neutron diffraction techniques [26], and high-energy x-ray scattering experiments [27] were used to carry out these phase transition studies. The electric field-induced transformations in NBT based materials were reviewed by Viola *et al* [28]. Piezoelectric ceramics find critical applications in ultrahigh precision positioning, where maintaining positional stability over prolonged periods is essential. Creep, characterized by a drift from the desired position during slow operations like scanning probe microscopy or atomic force microscopy, poses a significant challenge in these applications. To understand and mitigate creep effects, experiments examining the time-dependent electromechanical behavior of piezoelectric ceramics are necessary [29, 30]. While previous investigations have focused on the macroscopic strain response under varying electric field loading, the time-dependent electromechanical response under a constant electric field remains largely unexplored, especially in the context of lead-free ferroelectrics.

Creep behavior in ferroelectric ceramics has been extensively investigated for lead-based materials, such as PZT, where gradual ferroelectric domain switching processes have been associated with observed creep phenomena. Studies have been conducted under bipolar quasi-static electric fields with various hold times [31], as well as under unipolar constant electric fields [32], providing valuable insights into creep mechanisms. Similarly, for lead-free ferroelectric NBT-0.07BT, a cascade effect during electrical loading was observed, leading to significant creep behavior in both polarization and strain responses, associated with the transition from a nonergodic relaxor state (RE) to a state with long-range ferroelectric order [33]. Moreover, previous research on NBT-BT-KNN also revealed time-dependent variations through piezoresponse force microscopy, indicating a relaxation of electrically poled regions due to the reversibility of the field-induced ferroelectric phase as a function of KNN content [10]. However, there is a lack of macroscopic measurements concerning the time-dependence of strain and polarization for NBT-BT-KNN.

In this study, the macroscopic strain and polarization creep behavior of lead-free NBT-6BT-3KNN specimens were systematically characterized under constant electric field loads. The measurements revealed a continuous increase in polarization over time, attributed to the finite electrical resistivity at room temperature. To ensure accurate measurements, volume resistivity values were determined to eliminate the influence of leakage current on the polarization measurement. An Arrhenius-type exponential function was employed to fit the observed creep behavior, providing insights into the underlying mechanisms. The experimental setup involved maintaining a constant electric field for 900 s during both the increasing and decreasing periods. Comparative analysis of the results elucidated the phenomena, which can be explained by the gradual transition between the relaxor state (RE) and the ferroelectric state (FE). This transition was found to be a reversible process, occurring upon removal of the external electric field conditions. Understanding the time-dependent creep behavior of NBT-based lead-free ceramics is crucial for enhancing their performance and reliability in various actuator applications, particularly in ultrahigh precision positioning, where creep effects can significantly impact operational stability over prolonged periods.

2. Material and methods

Polycrystalline NBT-6BT-3KNN samples were produced by a solid oxide synthesis route; details of the production were reported previously [10, 34]. The primary powder was produced using the following powders with >99% purity from Alfa Aesar (Karlsruhe, Germany): Bi_2O_3, $BaCO_3$, K_2CO_3, Na_2CO_3, Nb_2O_5, and TiO_2. The raw powders were stoichiometrically weighed and ball milled for 24 h in ethanol and then dried for 48 h in a drying oven at 100 °C. After drying, the resulting powder was calcined in a two-step calcination process in alumina crucibles. The calcination was performed with a heating rate of 5 °C min^{-1}, a holding time of 2 h at 700 °C, a further heating at 5 °C min^{-1} to 800 °C, which was held for 3 h, followed by cooling at an uncontrolled rate to room temperature. After calcination, the calcined powder was ball milled for 24 h to produce powder with an average particle size of 1 μm. After drying for 48 h in a drying oven at 100 °C, the powders were subsequently pressed into green disks with a diameter of 10 mm under 70 MPa. Using a heating rate of 5 °C min^{-1}, sintering was carried out at 1100 °C for 3 h in covered alumina crucibles. Following this, the samples were cut to rectangular blocks of 4.25 mm × 4.25 mm × 2.7 mm with silver electrodes painted onto the top and bottom 4.25 mm × 4.25 mm surfaces. Figure 1(a) shows a sketch of the measurement setup, which was developed for electromechanical characterization under

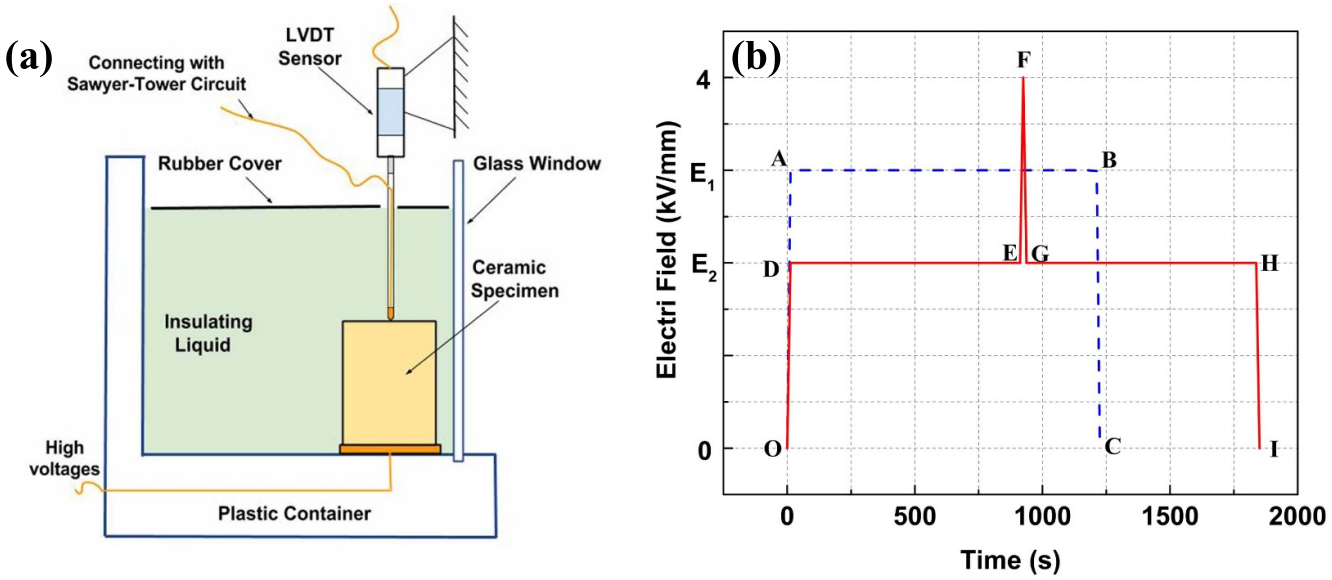

Figure 1. (a) Experimental setup for the electric field-induced creep measurement and (b) the two loading histories applied to the specimens.

high-voltage conditions. During measurement, the sample was immersed in a silicone oil bath (AB118663, abcr GmbH, Karlsruhe, Germany) to prevent arcing. A Sawyer–Tower circuit with a high input-resistance electrometer (6514, Keithley Instruments, Cleveland, OH) was used to measure polarization. The sample displacement was measured by means of a linear variable displacement transducer (Type W1T3, HBM, Darmstadt, Germany), which was used to determine the longitudinal strain. The electric field was applied by a high voltage power supply (HCB 15–30 000, F. u. G., Rosenheim, Germany). The setup is a part of our previous system used for monitoring the deformation of PZT specimens. The reproducibility and accuracy of this setup under high voltage test conditions have been previously validated [35].

The electromechanical behavior of the specimens was investigated under unipolar bias electric field loading with two distinct load histories. The experimental setup involved subjecting specimens to an electric field with loading and unloading rates of 0.16 kV mm^{-1} s^{-1}. Two distinct loading scenarios were explored, as depicted schematically in figure 1(b). In the first scenario, the sample was initially loaded to different electric field levels ($E_1 = 1$, 2, 3, or 4 kV mm^{-1}) and held constant for 1200 s (line AB in figure 1(b)). Subsequently, the sample was electrically unloaded back to 0 kV mm^{-1}. In the second scenario, the sample was initially loaded to a specific electric field level (E_2) at either 1, 2, or 3 kV mm^{-1} and held for 900 s (line DE). Following the hold time of 900 s, the sample was further loaded to 4 kV mm^{-1}, and immediately unloaded back to the original bias electric field, where it was held for another 900 s (line GH). Finally, after the second hold period, the sample was unloaded to 0 kV mm^{-1}. Throughout both loading scenarios, the longitudinal strain and polarization of the specimens were characterized to understand the time-dependent behavior during the complete loading process.

3. Results and discussion

In figure 2, the time-dependent behavior of both longitudinal strain and polarization is presented for the first loading scenario. The longitudinal strain (figure 2(a)) displays two distinct regimes: an immediate strain response upon initial electrical loading, followed by a gradual increase in strain with eventual saturation during the holding time. The strain experiences rapid growth during the initial loading period and subsequently exhibits a creep behavior under the constant electric field during the prolonged hold time. As the hold time progresses, the creep diminishes, and the strain eventually reaches a final saturation value. However, the polarization curves (figure 2(b)) do not exhibit saturation during the 1200 s hold time. This discrepancy is attributed to leakage current-induced charges accumulating in the reference capacitor of the Sawyer–Tower circuit, leading to a polarization drift measured by the electrometer. Importantly, such a drift is not observed in the strain response, reinforcing the belief that the time-dependent changes in polarization are predominantly influenced by leakage current. The Sawyer–Tower circuit assumes that the piezoelectric material behaves as an ideal capacitor with insulating properties, ensuring that the measured charge reflects polarization only and remains unaffected by charges caused by leakage. However, under high voltages during long hold times, the contribution of leakage current to measured charges becomes significant. To distinguish the polarization charge response from the influence of leakage current, a linear fitting operation was conducted on the linearly increasing sections of the measured charge per surface area toward the end of the linear part. In figure 2(b), the areas marked on each curve represent the sections where linear fitting was performed for the measured charge per specimen surface area under static loads. Specifically, the data obtained in the last 300 s were selected for the fitting, as the corresponding strain

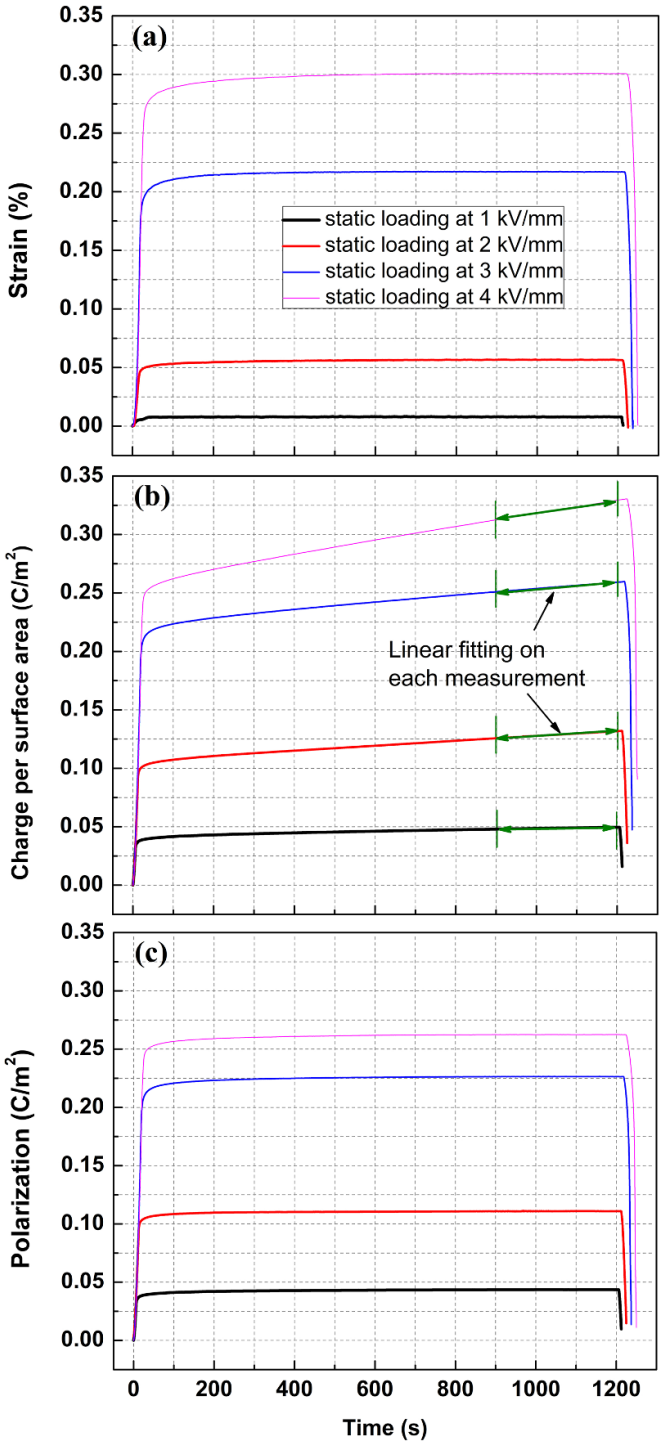

Figure 2. Longitudinal strain and polarization as a function of time: (a) measured strains; (b) measured charge per specimen surface area including charges from leakage; (c) polarization as a function of static electric fields.

in figure 2(a) indicates saturation in this regime, suggesting that the creep processes have concluded. Hence, the linear increase in the charge measurement during this period can be attributed solely to leakage currents and used to determine the polarization charge response.

Table 1. Volume resistivity under various static electric fields.

Electric field (kV mm^{-1})	Resistivity ρ (Ω m)
1	$(3.6 \pm 1.4) \times 10^{11}$
2	$(1.3 \pm 0.2) \times 10^{11}$
3	$(9.9 \pm 1.0) \times 10^{10}$
4	$(6.7 \pm 2.6) \times 10^{10}$

After performing this operation on all the four curves in figure 2(b), the values of slope in the fitted areas can be obtained. Then, the volume resistivity ρ was calculated by the following equation:

$$\rho = \frac{E}{m} \tag{1}$$

where E represents the static electric field applied and m is the slope of the linear fit. The experiments were repeated on three samples, each subjected to a single loading cycle, and the average results were recorded in table 1. To ensure accuracy, each resistivity value was obtained by averaging three sets of measured data from the three samples. Neglecting the leakage at the electrometer was justified due to a large input resistance (1 TΩ) of the Keithley 6514 used here. The volume resistivity is commonly regarded as approximately constant within a certain range of electric field or electric potential. The values of resistivity of PZT materials were reported as $\sim 10^{10}$ Ω m for PZT-4, and $\sim 10^{11}$ Ω m for PZT-5 H [36]. These values are given at room temperature and the variation of them depend on various factors, such as the composition as well as dopant type, concentrations in the material and defects too. For the specimens with the same composition used in our measurements, the observed volume resistivity values were found to exhibit a nonlinear dependence on the applied constant electric field. As shown in figure 3, the volume resistivity displayed an apparent decrease with increasing constant electric field. However, it is worth noting that the relatively large error in the resistivity measured at 1 kV mm^{-1} was attributed to the resolution of the experimental setup. At this relatively low electric field loading, the voltage signal measured by the Sawyer–Tower circuit was low, leading to a higher error in the three measured data points at 1 kV mm^{-1}.

Using the volume resistivity determined with equation (1), it is possible to correct the charge per specimen surface area for leakage, which allows us to obtain the time-dependent changes in polarization during the application of a bias electric field (figure 2(c)). The polarization can be calculated using the following equations:

$$P = P_{\mathrm{m}} - P_{\mathrm{l}} \tag{2}$$

$$P_{\mathrm{l}} = mt. \tag{3}$$

The polarization without the influence of leakage current (P), as shown in figure 2(c), can be calculated using the measured charge per specimen surface area (P_{m}) and the charge

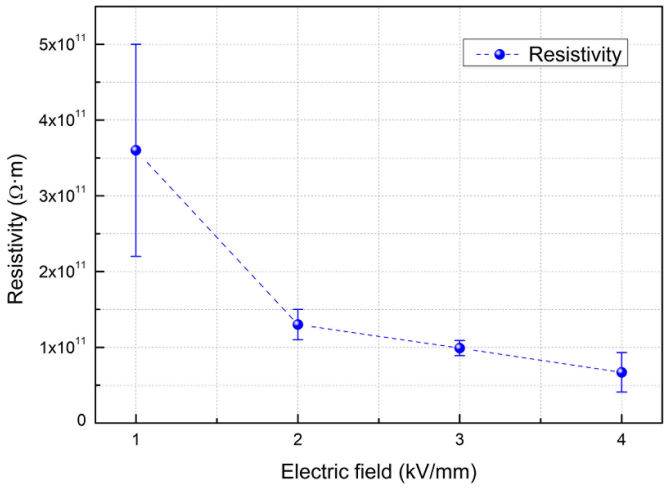

Figure 3. Resistivity values obtained from 4 static electric field loads.

per specimen surface area caused by leakage current (P_l), which can be obtained using equation (3) as the slope of the linear fit multiplied by time (t). Figure 2(c) illustrates the time-dependent behavior of polarization under four static electric fields, showing a similar trend to the strain curves, i.e. rapid growth initially, followed by saturation after a certain holding time. It is important to note that a constant leakage current for one test over the entire time is being assumed. As mentioned previously, the obtained results consist of two parts: (i) values measured under varying electric field load, and (ii) a creep response under static electric field load. Figure 4(a) provides an example of these two regimes in the measured strain. During the initial few seconds, both the strain and polarization increase owing to an electric field-induced transformation from a RE to a long-range ferroelectric order [10], a similar relaxor-to-ferroelectric phase transition induced by an external electric field has been reported in other NBT based solid solutions [37]. Beside the creep behavior attributed the phase transition, some studies argue that the O-vacancies and their related defects would induce dipoles which can align with the bias and heat combination loads [38]. It is believed that defect dipoles, i.e. the association of acceptor centers and oxygen vacancies, create an internal bias inside a domain and thus restrict the domain-wall motion. Ordered defect dipoles, alternatively the internal bias field, forming after poling could provide a strong restoring force for reversible domain-wall motion inside ferroelectrics, leading to a huge electric filed induced strain response [39]. However, more studies are needed to understand whether this O-vacancies motion or alignment of defect dipoles could contribute a creep response under a constant bias in NBT-BT-KNN ceramics.

Upon reaching the static state, creep strain (S_c) and creep polarization (P_c) were recorded at four constant electric fields, as shown in figures 4(b) and (c), respectively. The zero point on these graphs corresponds to the beginning of the hold time. Notably, the creep behavior is observed to be dependent on the magnitude of the applied static electric field. Surprisingly,

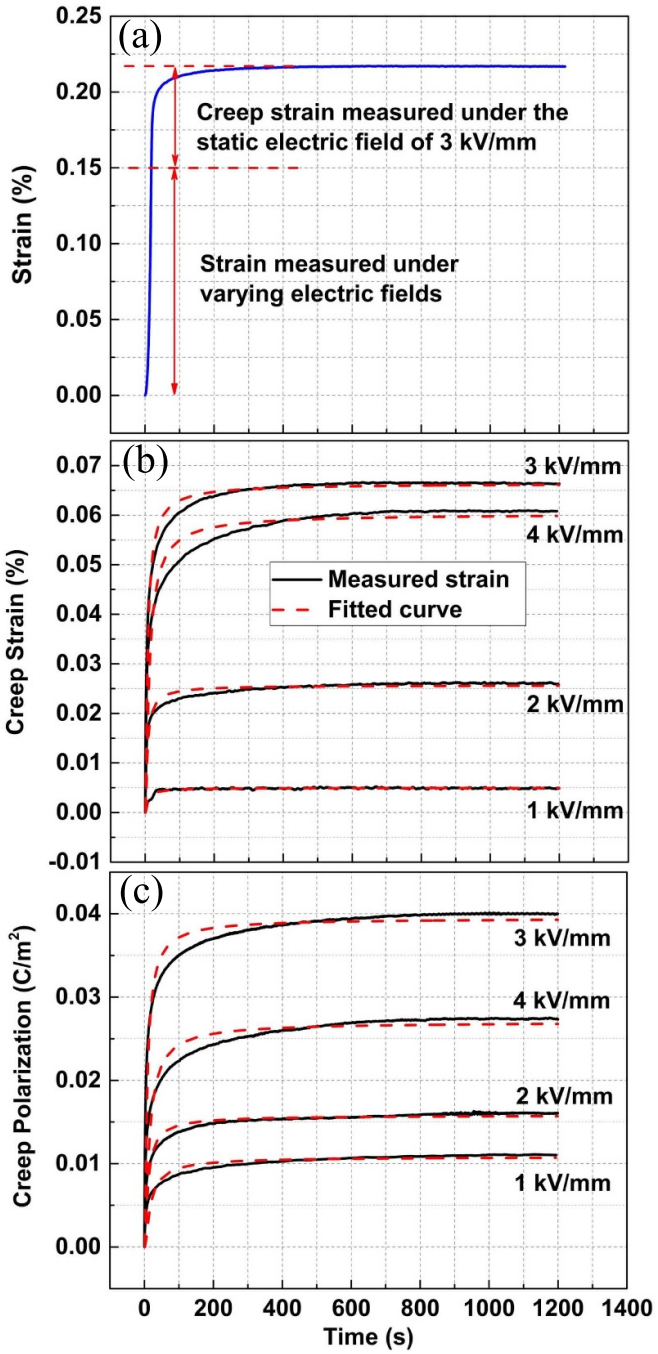

Figure 4. The creep behavior as a function of time: (a) two regimes of the obtained strains from 0 to 3 kV mm^{-1}; (b) measured creep strains along with the corresponded fitting curves; (c) measured creep polarization with the corresponded fitting curves.

S_c and P_c reach maximum values under the constant electric field of 3 kV mm^{-1}, rather than under the electric field of 4 kV mm^{-1}. The theory of exhaustion of switchable domains in PZT materials offers a potential explanation for this observation [40]. Higher applied electric field facilitate easier ferroelectric domain switching, thus influencing the observed creep. However, the total number of available domains for switching is limited. When the external constant electric field exceeds the coercive field, the creep of strain and

polarization decreases as a significant portion of switchable domains has been exhausted around the coercive field [31]. In this context, the creep behavior observed in our study can analogously be attributed to the 'exhaustion of phase transition'. At 1 kV mm^{-1}, a much lower S_c and P_c are obtained due to the low electric field's limited capacity to induce a substantial phase transition from the RE to the FE. As the static electric fields increase to the higher levels, both S_c and P_c show an upward trend, as the higher electric field leads to further induction of the RE-FE transition. However, once the electric field reaches 4 kV mm^{-1}, a significant amount of the available RE phase has already undergone transformation, which explains why S_c and P_c do not peak at this electric field magnitude.

To describe the creep behavior, exponential functions of Arrhenius type were used to fit the measured creep curves, expressed as equations (4) and (5):

$$S_c(t) = A_1 e^{-B_1/t} \tag{4}$$

$$P_c(t) = A_2 e^{-B_2/t} \tag{5}$$

where t is time, A_1 and A_2 are the magnitudes of creep response, and B_1 and B_2 are fitting coefficients representing the degree of difficulty in reaching saturation. The fitted curves are represented by dashed lines in figures 4(b) and (c), and the corresponding values of the four fitting parameters (A_1, A_2, B_1 and B_2) are listed in table 2. The values of A_1 and A_2 align with the 'exhaustion of phase transition' hypothesis discussed earlier. Moreover, B_1 and B_2 both reach their maximum values under the maximum applied electric field. Despite the potential errors in the measurement and fitting processes, the values of B_1 can still be categorized into two groups. The values of B_1 under constant electric fields of 1, 2, and 3 kV mm^{-1} belong to one group, where the electric fields are insufficient to fully transform the RE into FE. Therefore, the values of B_1 under these three electric fields exhibit a close resemblance. On the other hand, the second group includes only the value of B_1 under the applied field of 4 kV mm^{-1}, as it significantly surpasses the values observed under electric fields of 1, 2, and 3 kV mm^{-1}. It is noted that for NBT-BT-KNN materials, the minimum electric field required to achieve the saturation state is referred to as the poling field (E_{pol}) [41], which is typically exceeds 4 kV mm^{-1}. This is the reason why the maximum of electric fields in the reported work on NBT-BT-KNN were loaded to 6 kV mm^{-1} or even higher to reach a desired strain response [10, 34, 42]. It should be mentioned here, the E_{pol} of NBT-6BT-3KNN has been reported to be in the range of 4.5 and 5.5 kV mm^{-1} in previous studies. However, the specific value of E_{pol} can vary depending on various factors, including the processing conditions, composition of the material, and testing parameters such as temperature and electric field loading rate. E_{pol} of the ceramic in this study with the same composition as the reported ones is around 4.6 kV mm^{-1} (loading rate 10 mHz). Importantly, the lower frequency (10 mHz) used during the initial period of electric field increasing induced larger strain in NBT-6BT-3KNN, as demonstrated by Groh *et al* [43]. These findings collectively indicate that a state of complete polarization was achieved at 4 kV mm^{-1} during the prolonged hold time in our test, signifying that the RE was exhausted and fully transformed into the FE.

Table 2. The parameters obtained from the fitted creep curves.

Electric field (kV mm^{-1})	A_1	B_1	A_2	B_2
1	0.5×10^{-2}	6.5	1.1×10^{-2}	8.6
2	2.6×10^{-2}	4.9	1.6×10^{-2}	8.0
3	6.6×10^{-2}	5.3	3.9×10^{-2}	6.0
4	6.0×10^{-2}	9.3	2.7×10^{-2}	10.8

In consequence, the creep behavior at the high electric field differs from that at lower electric fields. The values of B_2 exhibit a similar tendency as B_1, indicating that both strain and polarization arise from the same creep mechanism. Before the exhaustion of the RE phase, the creep saturation is relatively easier to achieve. Once the RE to FE phase transition is complete or near completion, the creep mechanism is no longer solely dominated by this phase transition. Instead, it is influenced by a combined effect of FE domain creep due to switching and the aforementioned phase transition. Previous *in situ* high-energy x-ray synchrotron studies have demonstrated that during electrical loading, ferroelectric domains form perpendicular to the applied electric field direction [27]. Over a sufficiently long hold time, these domains may become mobile and contribute to the observed creep behavior. However, future research efforts are needed to provide a comprehensive explanation of these mechanisms and to improve the understanding of the time-dependent behavior including detailed modeling and additional experiments.

In the second loading scenario, each sample was subjected to a stepwise electric field loading process. Firstly, the sample was loaded to 1, 2, or 3 kV mm^{-1} and kept constant for 900 s during the electric field increasing period. After the 900 s hold time, the sample's electric field was increased to 4 kV mm^{-1}, followed by an immediate unload back to the original bias electric field, where it was held for another 900 s during the decreasing period. Finally, after the second hold time, the sample was unloaded to 0 kV mm^{-1}. The obtained polarizations and strains for this loading scenario are presented in figure 5. As discussed earlier, the leakage-induced charge has been subtracted from the data measured during holding, providing accurate polarization measurements. When the electric field load reaches a specific value (1, 2, 3, or 4 kV mm^{-1}), the polarization responses under dynamic load and static load exhibit evident differences. For instance, when the electric field reaches 3 kV mm^{-1} (figure 5(a)) and is held at that level, the measured polarization increases to 0.225 C m^{-2}, which is equivalent to the polarization at 3.5 kV mm^{-1} under monotonic electric field loading conditions. The strain responses show a similar trend in this experiment. In the following, we will show that the observation in this experiment is consistent with the previous discussion.

Under a constant electric field of 4 kV mm^{-1}, the polarization could reach or even surpass the polarization measured at E_{pol}, indicating completion of the electric field-induced phase

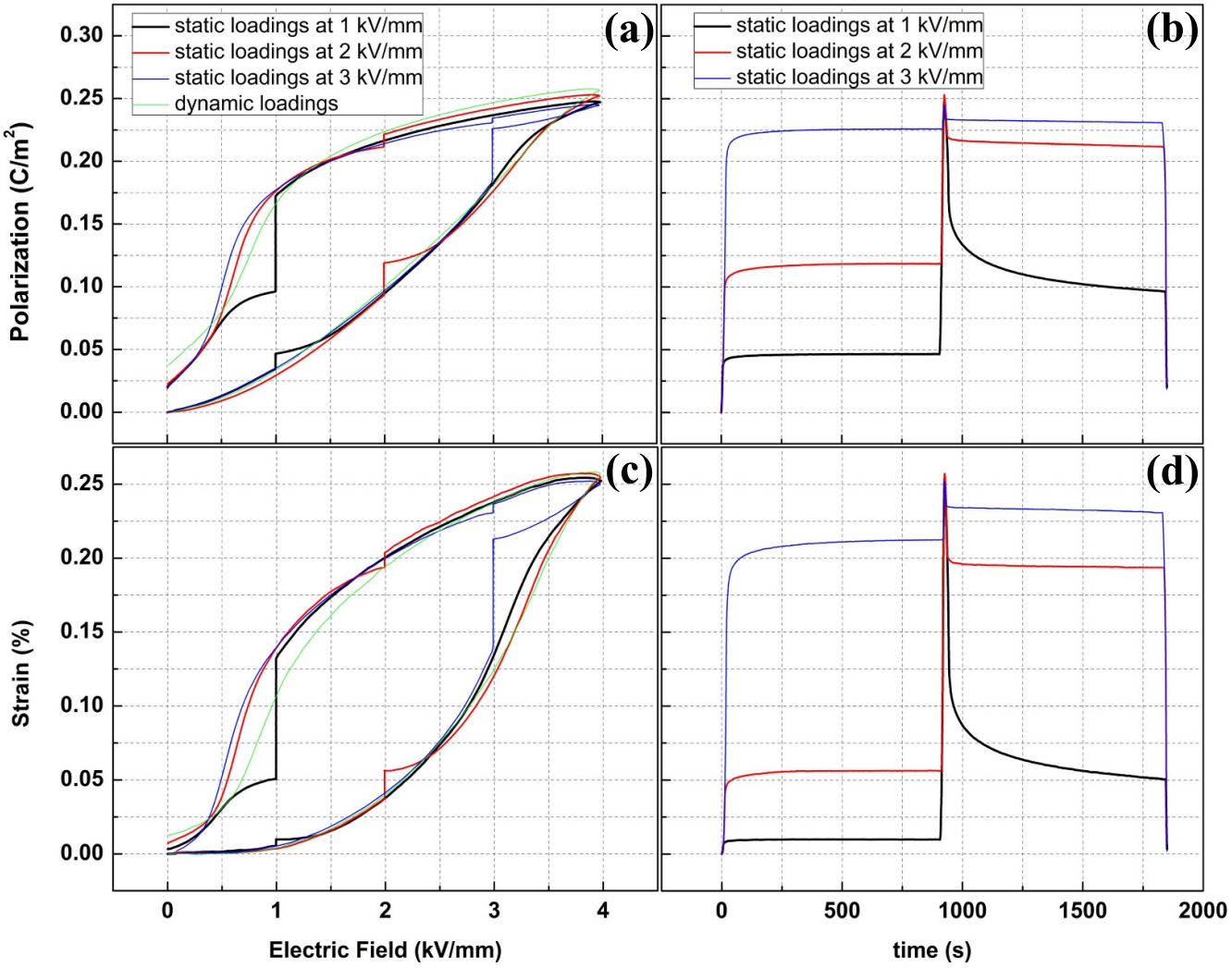

Figure 5. Polarization and strain responses as a function of applied electric fields: (a) polarization responses as a function of static and dynamic electric field loads; (b) electric field and time dependent polarization responses; (c) static and dynamic electric field and time dependent strain responses; (d) strain responses under constant electric fields loading plotted as a function of time.

transition during static loading at 4 kV mm^{-1}. The creep behavior under constant electric fields during the loading period, as depicted in figures 5(a) and (b), aligns well with the results in figure 2(c). During the initial hold time of 900 s, both polarization and strain exhibit apparent saturation behavior for each applied bias electric field level, as demonstrated in figures 5(b) and (d). In figure 5(a), while continuing the electrical loading from the previous bias field to 4 kV mm^{-1}, the polarization gradually increases to nearly the same value (0.25 C m^{-2}) for all three loading conditions. A similar trend is observed for strain values in figure 5(c). Upon unloading from 4 kV mm^{-1} to the respective bias electric field, a subsequent relaxation occurs, leading to time-dependent decreases in strain and polarization. Notably, 1 kV mm^{-1} shows the largest electromechanical relaxation during electrical field decreases to 1 kV mm^{-1} and holds there, whereas the measured relaxational strain and polarization at 2 and 3 kV mm^{-1} are much smaller. This distinction is attributed to the proximity to the critical reverse transformation field, where the long-range ferroelectric order to an ergodic RE. The critical electric field is defined as the inflection point in the unloading curve of the polarization-electric field response [41]. Consequently, as long as the unloading electric field remains higher than this critical electric field, the ferroelectric phase is retained Conversely, when the electric field decreases near or below the transition field, a reverse FE-RE transformation can occur. Similar to the largest creep obtained around the coercive field of PZT, this behavior can be attributed to the significant domain switching induced in that region [31, 32].

Compared with the NBT-BT-KNN discussed in this work, NBT-BT solid solutions without KNN exhibited the relaxor-to-ferroelectric transition induced by both electric field and mechanical stress [44]. This transition is not reversible unless a suitable temperature is reached ($T_{\text{FE-RE}}$). However, time dependence of the transition, especially loading rates dependence, were reported to strongly influence the poling field, coercive field, and remanent polarization, which is used to understand the dynamics of this transition [42, 45]. A gradual process with a cascade behavior can be observed when a constant electric field loading was applied on NBT-BT [33]. However,

this phenomenon was not found in this work even a similar experimental method was used and the origins of this difference remain controversial. The addition of KNN to NBT-BT reduces the long-range order of the material. And the cascade behavior in NBT-BT arises from the long-range order that facilitates its polarization, which is not present in BNT-BT-KNN.

4. Conclusion

This study focused on characterizing the creep behavior of polarization and strain in lead-free NBT-6BT-3KNN piezoceramics under constant electric fields. The measurement of polarization was carefully corrected to account for charge leakage-induced errors, allowing for the determination of approximate volume resistivity. Interestingly, the volume resistivity exhibited non-linear behavior under high electric field loading. Both polarization and strain responses showed significant time-dependence when subjected to a constant electric field. The primary mechanism behind the creep behavior of polarization and strain was attributed to the gradual phase transition between the RE and ferroelectric FE phases, which was found to be a reversible process. As a result, the electric field-induced creep behavior observed during constant electric field could be explained by the exhaustion of this phase transformation. Notably, large creep was observed only before the RE phase transformation reached saturation during the hold time. Once the RE phase transformation was nearly complete, higher electric fields did not induce larger creep nor drive the creep to reach saturation easily. This phenomenon was effectively described using an Arrhenius-type exponential function. Nevertheless, further investigation is needed to fully understand this behavior. For the electric decreasing process, prominent creep was observed near the critical field, where the electric field could no longer prevent the FE phase from transforming back to the RE phase.

Acknowledgments

D C and X C wish to thank the support by the Guangdong Basic and Applied Basic Research Foundation (Grant Nos. 2021A1515011810 and 2020A1515110220) and the State Key Laboratory of New Ceramic and Fine Processing Tsinghua University (No. KF202120). Mr. Mathieu Viry is thanked for assistance in designing the setup. K G W gratefully acknowledge financial support from the Deutsche Forschungsgemeinschaft under WE 4972/5-1 and WE 4972/8-1.

Conflict of interest

The authors declare no conflict of interest.

ORCID iD

Di Chen https://orcid.org/0000-0001-8181-2059

References

[1] Cao H and Evans A G 1993 *J. Am. Ceram. Soc.* **76** 890–6
[2] Schäufele A B and Heinz Härdtl K 1996 *J. Am. Ceram. Soc.* **79** 2637–40
[3] Es-Souni M, Kuhnke M, Piorra A and Solterbeck C H 2005 *J. Eur. Ceram. Soc.* **25** 2499–503
[4] Cross E 2004 *Nature* **432** 24–25
[5] Takenaka T, Maruyama K and Sakata K 1991 *Jpn. J. Appl. Phys.* **30** 2236–9
[6] Yao F Z *et al* 2016 *Adv. Funct. Mater.* **26** 1217–24
[7] Shibata K, Wang R, Tou T and Koruza J 2018 *MRS Bull.* **43** 612–6
[8] Rödel J, Webber K G, Dittmer R, Jo W, Kimura M and Damjanovic D 2015 *J. Eur. Ceram. Soc.* **35** 1659–81
[9] Waqar M, Wu H, Chen J, Yao K and Wang J 2022 *Adv. Mater.* **34** e2106845
[10] Dittmer R, Jo W, Rödel J, Kalinin S and Balke N 2012 *Adv. Funct. Mater.* **22** 4208–15
[11] Groh C, Franzbach D J, Jo W, Webber K G, Kling J, Schmitt L A, Kleebe H J, Jeong S J, Lee J S and Rödel J 2014 *Adv. Funct. Mater.* **24** 356–62
[12] Liu W and Ren X 2009 *Phys. Rev. Lett.* **103** 257602
[13] Saito Y, Takao H, Tani T, Nonoyama T, Takatori K, Homma T, Nagaya T and Nakamura M 2004 *Nature* **432** 84–87
[14] Rödel J, Jo W, Seifert K T P, Anton E-M, Granzow T and Damjanovic D 2009 *J. Am. Ceram. Soc.* **92** 1153–77
[15] Zhang S T, Kounga A B, Jo W, Jamin C, Seifert K, Granzow T, Rödel J and Damjanovic D 2009 *Adv. Mater.* **21** 4716–20
[16] Zhang S T, Kounga A B, Aulbach E, Ehrenberg H and Rödel J 2007 *Appl. Phys. Lett.* **91** 112906
[17] Jo W, Granzow T, Aulbach E, Rödel J and Damjanovic D 2009 *J. Appl. Phys.* **105** 094102
[18] Lv X, Wu J and Zhang X 2020 *Chem. Eng. J.* **402** 126215
[19] Song G, Zhang F, Liu F, Liu Z and Li Y 2021 *J. Am. Ceram. Soc.* **104** 4049–57
[20] Zhang Y, Liang G, Tang S, Peng B, Zhang Q, Liu L and Sun W 2020 *Ceram. Int.* **46** 1343–51
[21] Schmitt L A, Kling J, Hinterstein M, Hoelzel M, Jo W, Kleebe H J and Fuess H 2011 *J. Mater. Sci.* **46** 4368–76
[22] Schmitt L A, Hinterstein M, Kleebe H-J and Fuess H 2010 *J. Appl. Crystallogr.* **43** 805–10
[23] Kling J, Tan X, Jo W, Kleebe H-J, Fuess H and Rödel J 2010 *J. Am. Ceram. Soc.* **93** 2452–5
[24] Daniels J E, Jo W, Rödel J, Honkimäki V and Jones J L 2010 *Acta Mater.* **58** 2103–11
[25] Fancher C M, Iamsasri T, Blendell J E and Bowman K J 2013 *Mater. Res. Lett.* **1** 156–60
[26] Hinterstein M, Knapp M, Hölzel M, Jo W, Cervellino A, Ehrenberg H and Fuess H 2010 *J. Appl. Crystallogr.* **43** 1314–21
[27] Daniels J E, Jo W, Rödel J and Jones J L 2009 *Appl. Phys. Lett.* **95** 032904
[28] Viola G, Tian Y, Yu C, Tan Y, Koval V, Wei X, Choy K-L and Yan H 2021 *Prog. Mater. Sci.* **122** 100837
[29] Habibullah H, Pota H R, Petersen I R and Rana M S 2013 *IEEE Trans. Nanotechnol.* **12** 1125–34
[30] Croft D, Shed G and Devasia S 2001 *J. Dyn. Syst. Meas. Control* **123** 35–43

[31] Zhou D and Kamlah M 2005 *J. Appl. Phys.* **98** 104107
[32] Liu Q D and Huber J E 2006 *J. Eur. Ceram. Soc.* **26** 2799–806
[33] Chen D, Ayrikyan A, Webber K G and Kamlah M 2017 *J. Appl. Phys.* **121** 114106
[34] Zhang S T, Kounga A B, Aulbach E, Granzow T, Jo W, Kleebe H-J and Rödel J 2008 *J. Appl. Phys.* **103** 034107
[35] Chen D and Kamlah M 2015 *Rev. Sci. Instrum.* **86** 113707
[36] Berlincourt D, Krueger H and Near C 2000 Properties of Morgan electro ceramic ceramics *Technical Publication TP-226* (Morgan Electro Ceramics)
[37] Jing R, Zhang L, Hu Q, Alikin D O, Shur V Y, Wei X, Zhang L, Liu G, Zhang H and Jin L 2022 *J. Materiomics* **8** 335–46
[38] Warren W L, Vanheusden K, Dimos D, Pike G E and Tuttle B A 1996 *J. Am. Ceram. Soc.* **79** 536–8
[39] Liu Y-X, Thong H-C, Cheng Y-Y-S, Li J-W and Wang K 2021 *J. Appl. Phys.* **129** 024102
[40] Viola G, Chong K B, Guiu F and Reece M J 2014 *J. Appl. Phys.* **115** 034106
[41] Zhang H B, Groh C, Zhang Q, Jo W, Webber K G and Rödel J 2015 *Adv. Electron. Mater.* **1** 1500018
[42] Jo W, Dittmer R, Acosta M, Zang J, Groh C, Sapper E, Wang K and Rödel J 2012 *J. Electroceram.* **29** 71–93
[43] Groh C, Jo W and Rödel J 2014 *J. Appl. Phys.* **115** 234107
[44] Martin A, Khansur N H, Riess K and Webber K G 2019 *J. Eur. Ceram. Soc.* **39** 1031–41
[45] Martin A, Uršič H, Rojac T and Webber K G 2019 *Appl. Phys. Lett.* **114** 052901
[46] Chen D 2017 *Experimental Investigation of Strain Distributions and Polarization in Lead-Based and Lead-Free Ferroelectrics* (Karlsruher Institut für Technologie (KIT))